Efficient non-resonant energy transfer in Nd^{3+} - Yb^{3+} codoped Ba-Al-metaphosphate glasses

Atul D. Sontakke, Kaushik Biswas, R. Sen, K. Annapurna[†]

Glass Science and Technology Section, Central Glass and Ceramic Research Institute
(*Council of Scientific and Industrial Research*),
196, Raja S.C. Mullick Road, Kolkata – 700 032, India.

[†]Corresponding author: annapurnak@cgcri.res.in

ABSTRACT

An efficient $Nd^{3+} \rightarrow Yb^{3+}$ energy transfer in a new series of alkali-free barium-alumino-metaphosphate glasses with a transfer efficiency reaching up to 95% has been reported here. It is due to the effective phonon assistance arising with the excellent matching of the present host phonon energy with the energy mismatch between Nd^{3+} ($^4F_{3/2}$) and Yb^{3+} ($^2F_{5/2}$) excited levels. The energy transfer microparameters for $Nd^{3+} \rightarrow Yb^{3+}$ forward and back energy transfer are estimated from the spectral data analysis. A parameter, Φ_{ET} ($= C_{DA}^{Nd-Yb} / C_{DA}^{Nd-Nd}$) is proposed as a quantitative measure of sensitization ability per unit loss of the donor. The parameter is found to be highest for the presently reported barium-alumino-metaphosphate glasses.

OCIS codes: 140.3380, 140.5680, 260.2160, 160.2750

1. INTRODUCTION

The systems operating at one micron based on Yb^{3+} emission sensitised by Nd^{3+} codoping have been drawing much attention because of their potential applications in solar energy concentrators and high energy lasers [1-11]. The multiple absorption bands of Nd^{3+} in the regions of UV-visible-NIR could facilitate an effective utilization of solar spectrum and thus providing a variety of pumping options for Yb^{3+} ions to fluoresce at around 1 μm, which lies just above the band gap of Si (~1.1 eV). Apart from this, the broadband emission of Yb^{3+} ions along with a reasonable emission cross-section having high storage capacity opens up greater opportunity for ultra-short pulsed lasers in advanced applications including thermonuclear fusion reactions [12, 13]. In this context, the primary requirement lies in the selection of an appropriate host possessing efficient $Nd^{3+} \rightarrow Yb^{3+}$ energy transfer, which has become a subject of interest for many researchers.

For $Nd^{3+} \rightarrow Yb^{3+}$ system, the energy transfer could be a resonant or a non-resonant (phonon assisted) process depending on the spectral overlap between donor's emission and acceptor's absorption. Recently, a resonant $Nd^{3+} \rightarrow Yb^{3+}$ energy transfer has been reported in a ferroelectric $Sr_{0.6}Ba_{0.4}Nb_2O_6$ laser crystal with an efficiency reaching up to 50% for 10 at% of acceptor concentration [10]. However, for most of the systems studied, the energy transfer occurs through the phonon assistance owing to the spectral mismatch between Nd^{3+} - Yb^{3+} ions [1-9]. A good matching of host phonon energy (E_{ph}) with the energy difference between excited levels $^4F_{3/2}$ of Nd^{3+} and $^2F_{5/2}$ of Yb^{3+} ions could result in an efficient phonon assisted energy transfer. Such an observation has been made in $YAl_3(BO_3)_4$ non-linear laser crystal having maximum phonon energy of 1030 cm^{-1}, which is almost matching with the Nd^{3+} - Yb^{3+} energy difference of 1070 cm^{-1}, yielding an energy transfer efficiency more than 90% [14, 15]. Thus the selection of an appropriate host material has become more crucial for the Nd^{3+}-Yb^{3+} codoped system in demonstrating an efficient sensitised luminescence. In this

regard, the metaphosphate glasses are of interest due to their phonon energy laying around 1000 - 1200 cm^{-1} in combination with the chain like glass network providing superior doping ability [16]. From our initial work on Nd^{3+} doped metaphosphate glasses, it was found that the alkali-free barium-alumino-metaphosphate glasses possess better water resistivity, higher energy storage capacity, optimum emission cross-section and other spectroscopic properties comparable to the commercial laser glasses [17]. This has led us to investigate the spectroscopic properties of Nd^{3+} - Yb^{3+} codoped barium-alumino-metaphosphate glasses because of their promising prospectives as solar energy concentrators and high power lasers. In the present work, a detailed analysis of energy transfer mechanism between Nd^{3+} and Yb^{3+} ions codoped in barium-alumino-metaphosphate glasses has been carried out for a wide range of acceptor concentration. Both photoluminescence spectra and donor fluorescence decay analysis have been used to evaluate the energy transfer efficiency along with transfer microparameters and discussed in comparison with other Nd^{3+} - Yb^{3+} codoped materials.

2. EXPERIMENTAL

Nd^{3+} - Yb^{3+} codoped barium-alumino-metaphosphate glasses having chemical compositions in mol% (99-x) (20.95 BaO - 11.72 Al_2O_3 - 56.12 P_2O_5 - 6.79 SiO_2 - 3.91 B_2O_3 - 0.51 Nb_2O_5) + 1.0 Nd_2O_3 + x Yb_2O_3 (x = 0, 0.05, 0.1, 0.5, 1.0, 3.0, 6.0, 9.0) were prepared by employing the melt quenching technique. All the developed glasses have been labelled as BAP-Nd, BAP-NdYb005, - - -, BAP-NdYb90 based on the Yb^{3+} concentration. Reagent grade metaphosphate chemicals such as $Ba(PO_3)_2$ and $Al(PO_3)_3$, and rare earth oxides Nd_2O_3, Yb_2O_3 with 99.99% purity from Alpha-Aesar were used as starting materials for the glass preparation. Thoroughly mixed chemical batches were sintered at 350°C for 6 h to reduce the surface absorbed moisture and make pre-reacted batch. Each sintered batch was then melt at

1350°C in high purity quartz crucibles for 1 hour with intermittent stirrings to ensure homogeneity and later each of the melts was cast onto preheated graphite moulds. The cast glass samples were subsequently transferred to a precise temperature controlled annealing furnace kept at 550°C for annealing to relieve thermal stresses followed by a slow cooling to the room temperature. During glass melting process, the relative atmospheric humidity was maintained below 40%. The annealed glasses were then cut and polished in the form of rectangular plates in dimensions of $15 \times 20 \times 2$ mm^3 for further characterization.

The optical absorption spectra of glasses were recorded on a UV-Vis spectrophotometer (Model: Lambda20, Perkin-Elmer) in the wavelength range of 200 - 1100 nm. The Photoluminescence and decay measurements were carried out on a Fluorescence spectrophotometer (Model: Quantum Master-enhanced NIR, from Photon Technologies International) fitted with double monochromators on both excitation and emission channels. The instrument is equipped with LN_2 cooled gated NIR photo-multiplier tube (Model: NIR-PMT-R1.7, Hamamatsu) as detector for acquiring the data from both steady-state spectra and phosphorescence decay. For performing decay measurements on the same equipment, a 60W Xenon flash lamp was employed as an excitation source. All the measurements were carried out by placing the samples at 60^0 to the incident beam and the signals were collected from the same surface at right angle to the incident beam.

3. THEORETICAL BACKGROUND

Sensitized luminescence in rare earth ions doped materials can be defined as a phenomenon where an activator ion (energy acceptor) is enabled to fluoresce by the aid of a different kind of ion, termed as sensitizer (energy donor) upon the absorption of light followed by subsequent radiation less energy transfer by the later. The energy transfer among donor-acceptor takes place through the coupling interactions. These interactions can be

electrostatic multipole interactions such as dipole-dipole, dipole-quadrupole, quadrupole-quadrupole, etc., or the exchange interactions [18]. Among them, the dipole-dipole interactions have long-range influence and are accountable for the energy transfer in most of the cases. Previous investigations have established that the dipole-dipole interactions are responsible for the energy transfer in Nd^{3+} - Yb^{3+} ions [2-11]. According to Forster-Dexter theory, the energy transfer probability (P_{ET}) depends on the spectral overlap integral resulting from donor's emission and acceptor's absorption [18]. However, for certain donor-acceptor system, the spectral overlap may be poor owing to the non-resonant transitions. In such cases, the host lattice vibrational energy (phonon) contribute to energy transfer by bridging the energy difference and the energy transfer probability can be estimated using the phonon modified spectral overlap integral given as [3]

$$P_{ET} \propto I(E_{ph}) = \frac{e^{E_{ph}/k_B T}}{e^{E_{ph}/k_B T} - 1} \int \frac{f_D(E - E_{ph}) f_A(E)}{E^2} dE , \tag{1}$$

where, $f_D(E)$ and $f_A(E)$ are the line-shape functions of donor's emission and acceptor's absorption respectively, and E_{ph} is the host phonon energy. This relation usually provides an estimation of non-resonant energy transfer processes, like $Nd^{3+} \rightarrow Yb^3$ in particular host matrix. A more quantitative measure for Nd^{3+} to Yb^{3+} energy transfer can be obtained through the energy transfer efficiency η_{ET}, which can be calculated from the spectral data using the expression [10, 14]

$$\eta_{ET} = \frac{\eta_{Yb}^{-1} \int_{850nm}^{1100nm} I_{Em}^{Yb}(\lambda) d\lambda}{\eta_{Nd}^{-1} \left(1 + \frac{\beta_{^4I_{13/2}} + \beta_{^4I_{15/2}}}{\beta_{^4I_{9/2}} + \beta_{^4I_{11/2}}} \right) \int_{850nm}^{1100nm} I_{Em}^{Nd}(\lambda) d\lambda + \eta_{Yb}^{-1} \int_{850nm}^{1100nm} I_{Em}^{Yb}(\lambda) d\lambda} , \tag{2}$$

where, η_{Nd} (≈0.76) and η_{Yb} (≈0.95) are the quantum yields of Nd^{3+} and Yb^{3+} ions respectively in present glasses, $I(\lambda)$ is the emission intensity and β is the branching ratio. Also, the donor

(Nd^{3+}) luminescence decay time in codoped samples can provide the energy transfer efficiency by adopting the relation [1, 11]

$$\eta_{ET} = 1 - \frac{\tau_{Nd-Yb}}{\tau_{Nd}}, \tag{3}$$

where, τ_{Nd} and $\tau_{Nd\text{-}Yb}$ are the Nd^{3+} fluorescence decay time for singly and codoped samples respectively. The donor fluorescence decay kinetics has another importance in retrieving the key information regarding donor-acceptor coupling interactions and their energy transfer microparameters with the aid of certain theoretical models. At low donor concentration, the energy transfer follows direct donor to acceptor path and the Inokuti - Hirayama model can be used for decay analysis [19]

$$I(t) = I_0 \exp\left[-\frac{t}{\tau_0} - \frac{4\pi}{3} N_A \Gamma\left(1 - \frac{3}{s}\right) (C_{DA} t)^{3/s} \right], \tag{4}$$

where, N_A is acceptor ion concentration, Γ is Euler's gamma function, s is electrostatic interaction parameter (s = 6 for dipole-dipole interactions) and C_{DA} is the microscopic energy transfer parameter between donor and acceptor. C_{DX} *(X = A* or *D)* is an intrinsic parameter of respective host material and it can be estimated using the relation [17, 20]

$$C_{DX} = \frac{3c}{8\pi^4 n^2} \int \sigma_{em}^{D}(\lambda) \sigma_{abs}^{X}(\lambda) d\lambda, \tag{5}$$

where, c is the velocity of light in vacuum, n is the refractive index and $\sigma_{em}^{D}(\lambda)$, $\sigma_{abs}^{X}(\lambda)$ are the emission and absorption cross-sections of donor and acceptor/donor respectively. However, if the energy transfer is phonon assisted, it has to be taken into account while calculating the energy transfer microparameters using above relation. It can be done by constructing the Stokes phonon sidebands to the absorption and emission cross section spectra with the help of exponential law proposed by Auzel as given below [21, 22]

$$\sigma_{Stokes} = \sigma_{elect} \exp(-\alpha_S \Delta E), \tag{6}$$

where, ΔE is the energy mismatch between electronic and vibronic transitions and α_S is the host dependent parameter for Stokes transitions represented as

$$\alpha_S = (h\nu_{\max})^{-1}\left(\ln\{(\overline{N}/S_0)[1-\exp(-h\nu_{\max}/kT)]\}-1\right), \tag{6a}$$

where, $\overline{N}$ is the number of phonons required for bridging the energy gap, S_0 is the electron-phonon coupling constant (≈0.04), $h\nu_{max}$ is the maximum phonon energy of host, k is Boltzmann constant and T is temperature.

The C_{DD} term defines the donor-donor energy migration microparameter. At high donor concentration, the donor to acceptor energy transfer takes place through donor-donor energy migration mechanism. If $C_{DD} > C_{DA}$, the migration occurs through hopping mechanism and the Burshtein model can be applied for decay analysis given by [17]

$$I(t) = I_0 \exp\left[-\frac{t}{\tau_0} - \frac{4\pi}{3} N_A \Gamma\left(1-\frac{3}{s}\right)(C_{DA}t)^{3/s} - W_m t\right], \tag{7}$$

where W_m is called as migration parameter.

Apart from the donor-acceptor energy transfer and donor-donor energy migration, luminescence self-quenching through cross-relaxation mechanism among nearest neighbouring donor ions is an important factor in view of the sensitized luminescence [23]. For Nd^{3+} ions, the self-quenching occurs through $^4F_{3/2} \rightarrow {}^4I_{15/2} : {}^4I_{9/2} \rightarrow {}^4I_{15/2}$ transitions and is estimated by a self-quenching microparameter, C_{DA}^{Nd-Nd} [17]. The C_{DA}^{Nd-Nd} is considered to be a loss term as its higher value signifies faster depopulation of the $^4F_{3/2}$ level of Nd^{3+} ions by means of cross-relaxation mechanism before actual transfer to Yb^{3+} ions [5]. So, in order to obtain an efficient sensitised luminescence from Yb^{3+} ions, the $Nd^{3+} \rightarrow Yb^{3+}$ energy transfer microparameter, C_{DA}^{Nd-Yb} should be much higher than the $Nd^{3+} \rightarrow Nd^{3+}$ self-quenching

microparameter, C_{DA}^{Nd-Nd}. This led us to introduce a performance factor, (Φ_{ET}) as a measure of sensitization ability per unit loss, which can give a more quantitative understanding of sensitised luminescence for a codoped system and is given by

$$\Phi_{ET} = \frac{C_{DA}^{Nd-Yb}}{C_{DA}^{Nd-Nd}}. \quad (8)$$

4. RESULTS AND DISCUSSION

A. Absorption and Sensitised Luminescence Spectra

The room temperature UV-Visible optical absorption spectra of Nd^{3+} - Yb^{3+} codoped Ba-Al-metaphosphate glasses with varied Yb^{3+} concentrations are presented in Fig. 1. The spectra have revealed various characteristic absorption bands from Nd^{3+} and Yb^{3+} ions, which have been assigned appropriately based on their respective peak positions. While Nd^{3+} ions display multiple absorption transitions from ground state to different excited states of $4f^3$ configuration, Yb^{3+} ions show a broad absorption resulting due to the transitions from ground state multiplet, $^2F_{7/2}$ to $^2F_{5/2}$ excited state multiplet of $4f^{13}$ configuration with its peak maximum at 975 nm wavelength. The intensity of absorption peak at 975 nm is linearly increased with an increase in Yb^{3+} concentration following the Beer's law but no significant variations are observed in absorption peak intensities of Nd^{3+} ions, as the Nd^{3+} concentration is kept constant at 1 mol% in all the glasses. Also, it is clear from the figure that, Nd^{3+} ions absorb significantly in the visible with a strong absorption at around 584 nm ($^4I_{9/2} \rightarrow {}^4G_{5/2,}$ $^2G_{7/2}$), which especially falls on the peak maximum of solar spectrum. Apart from this, another strong absorption at around 806 nm ($^4I_{9/2} \rightarrow {}^4F_{5/2}$) is found to be ideal one for the laser diode excitation. We examined the energy transfer kinetics between Nd^{3+} and Yb^{3+} ions

by excitation of Nd^{3+} ions under both 584 nm as well as 806 nm wavelengths and found no significant dependence of excitation wavelength on the energy transfer parameters.

Figure 2 presents the photoluminescence spectra of Nd^{3+} - Yb^{3+} codoped barium-alumino-metaphosphate glasses on Nd^{3+} excitation at 806 nm for a wide range of Yb_2O_3 concentration from 0 to 9 mol%. For Nd^{3+} singly doped glass BAP-Nd, intense emission bands peaking at 887 nm, 1058 nm and 1324 nm have been assigned to the electronic transitions of $^4F_{3/2} \rightarrow {}^4I_{9/2,\ 11/2\ \text{and}\ 13/2}$ respectively. An additional broad emission at around 1 μm appeared on codoping with the Yb^{3+} ions is due to $^2F_{5/2} \rightarrow {}^2F_{7/2}$ transition of Yb^{3+} ions. Inset of Fig. 2 shows the variation of emission intensities of both Nd^{3+} and Yb^{3+} ions as a function of Yb_2O_3 concentration. The Nd^{3+} emission intensity decreases continuously with an increase in Yb^{3+} ion concentration and almost vanishes for the glasses with 3 mol% Yb_2O_3 and above due to non-radiative energy transfer from Nd^{3+} to Yb^{3+} ions following the path (Nd^{3+}: $^4F_{3/2} \rightarrow Yb^{3+}$: $^2F_{5/2}$). However, the Yb^{3+} emission intensity increases up to 3 mol% Yb_2O_3 concentration and then diminishes for any further increase in its concentration. The decrease in Yb^{3+} emission intensity at higher concentration may be due to the energy migration among Yb^{3+} ions, which subsequently results in the energy loss to quenching centres. The quenching is also possible due to $Nd^{3+} \leftarrow Yb^{3+}$ energy back-transfer. Apart from this, a change in the spectral shape of Yb^{3+} emission has been detected at higher Yb^{3+} concentration and is attributed to the reabsorption of radiative emission by unexcited Yb^{3+} ions.

B. Energy Transfer Probability and Host Phonon Influence

Figure 3 presents the emission and absorption cross sections of $^4F_{3/2} \rightarrow {}^4I_{9/2}$ transition of Nd^{3+} and $^2F_{7/2} \rightarrow {}^2F_{5/2}$ transition of Yb^{3+} ions respectively. The spectra depict a poor spectral overlap owing to the energy difference that exists between the excited state energy levels of $^4F_{3/2}$ (Nd^{3+}) and $^2F_{5/2}$ (Yb^{3+}). A partial energy level diagram has been plotted for the

dopant ions in the present host from their measured absorption spectral positions and is shown in inset of Fig.3. It can be seen that the $^4F_{3/2}$ level of Nd^{3+} is slightly elevated from the $^2F_{5/2}$ level of Yb^{3+} ions with an energy difference (ΔE) of around 1150 cm^{-1}, suggesting the energy transfer between donor and acceptor ions may not be resonant but of host phonon assisted. To get a clear understanding of the appropriate phonons required for efficient energy transfer, the energy transfer probability (P_{ET}) have been calculated for different phonon energies using Eq. (1). Figure 4(a) furnishes the variation of energy transfer probability (P_{ET}) as a function of phonon energy (E_{ph}) in the range of 300 to 1300 cm^{-1}. It is observed that the energy transfer probability increases with the increase in phonon energy and attains a maximum for the phonons having energy in the range of 900 - 1200 cm^{-1}. This exactly matches with the phonon energy of presently studied barium-alumino-metaphosphate glasses as depicted in the FTIR reflectance spectra in Fig. 4(b); exhibiting strong absorption bands at 920 cm^{-1} and 1110 cm^{-1} due to asymmetric vibrational transitions of (P-O-P) group and non-bridging ($P\text{-}O^-$) group respectively [24].

C. $Nd^{3+} \rightarrow Yb^{3+}$ Energy Transfer Efficiency and Microparameters

The energy transfer efficiency, η_{ET} has been estimated for all the codoped glasses by using Eqs. (2) and (3). Figure 5 shows the variation of energy transfer efficiency for $Nd^{3+} \rightarrow Yb^{3+}$ energy transfer as a function of Yb_2O_3 concentration. From this figure, it is clear to notice that the energy transfer efficiency estimated from spectral data is in close agreement with that derived from donor fluorescence decay kinetics. At low acceptor concentration, the energy transfer efficiency exhibits a rapid enhancement, which gets retarded for the glasses having Yb_2O_3 concentration above 1 mol%. This trend of energy transfer efficiency at higher Yb^{3+} concentration may be due to the saturation of energy transfer owing to relatively high acceptor concentration. The fluorescence decay curves of Nd^{3+} emission at 887 nm on 806

nm excitation are presented in Fig. 6. For BAP-Nd glass, the decay profile is nearly single exponential with the decay time of 283.6 μsec; however, it becomes non-exponential for codoped samples owing to the non-radiative energy transfer from Nd^{3+} to Yb^{3+} ions. The measured decay time (τ) and Nd^{3+} - Yb^{3+} energy transfer rate (W_{ET}) for all samples are listed in Table I along with the energy transfer efficiency (η_{ET}) [4, 25]. The obtained energy transfer efficiency from both emission data and donor luminescence decay are found to be more than 95% for BAP-NdYb90 glass demonstrating an efficient energy transfer in present host.

For designing a laser device based on sensitised luminescence, it becomes essential to understand the exact nature of coupling interactions (dipole-dipole in this case [17, 25]) between donor-acceptor as well as the microscopic energy transfer parameters, C_{DA} among donor-acceptor, donor-donor and other quenching centres [23]. This can be done by analysing the donor luminescence decay profiles with the help of certain theoretical models. Generally, the donor-acceptor energy transfer takes place through different mechanisms such as direct energy transfer or donor-donor migration assisted energy transfer, which could further subdivided in diffusion limited or hopping limited migration. Thus the selection of an appropriate theoretical model is considered to be playing a crucial part in the decay analysis. The classical Inokuti-Hirayama model, Eq. (4) is applicable at low donor concentration; but at Nd_2O_3 concentration as high as 1 mol%, migration effect can not be ruled out [17, 25]. If the donor-acceptor energy transfer microparameter C_{DA}^{Nd-Yb} is less than the donor-donor energy migration microparameter C_{DD}^{Nd-Nd}; the migration is supposed to occur through the hopping mechanism otherwise through diffusion mechanism [25]. The value of C_{DA}^{Nd-Yb} can be obtained from the spectral overlap function. Figure 7 shows the emission and absorption cross section spectra for Nd^{3+} and Yb^{3+} ions with respective phonon sidebands drawn using the exponential law of Auzel in Eq. (6). From this phonon modified spectral overlap, the

energy transfer microparameter C_{DA}^{Nd-Yb} equals to 1.65×10^{-39} $cm^6 s^{-1}$ has been obtained for $Nd^{3+} \rightarrow Yb^{3+}$ energy transfer by using Eq. (5), which is close to the value reported for lithium-lanthanum-metaphosphate glass (1.6×10^{-39} $cm^6 s^{-1}$) [26]. The donor-donor energy migration microparameter, C_{DD}^{Nd-Nd} for present barium-alumino-metaphosphate glass is found to be equal to 3.8×10^{-39} $cm^6 s^{-1}$ from our previous studies [17, 25]. Thus it is clear that the $C_{DA}^{Nd-Yb} < C_{DD}^{Nd-Nd}$ suggesting hopping migration among donors. Figure 8 represents the Nd^{3+} luminescence decay curve of BAP-NdYb05 sample along with a theoretical fitting made by Eq. (7) by considering $C_{DA}^{Nd-Yb} = 1.65 \times 10^{-39}$ $cm^6 s^{-1}$, which showed an excellent correlation with the experimental data confirming the hopping migration assisted energy transfer in present glasses. Further, the close matching of energy transfer microparameter value obtained from experimental decay kinetics and phonon modified spectral overlap model substantiates the assumption of phonon assistance in energy transfer mechanism.

Basically, the energy transfer microparameter C_{DA}^{Nd-Yb} signifies the ability of energy transfer from Nd^{3+} to Yb^{3+} in a particular host material and is an intrinsic property of that host. Table II presents the $Nd^{3+} \rightarrow Yb^{3+}$ energy transfer microparameter values for different host materials along with the respective Nd^{3+} self-quenching microparameter (C_{DA}^{Nd-Nd}) for a comparison. The data in Table II indicates that the borate hosts are most efficient for Nd^{3+} to Yb^{3+} energy transfer, which may be due to their higher phonon energies [3]. However, the higher host phonon energy also increases the non-radiative energy loss of $^4F_{3/2}$ level of Nd^{3+} due to multi-phonon relaxation resulting in lower quantum yield [27]. Additionally, the energy transfer microparameter for Nd^{3+} self-quenching (C_{DA}^{Nd-Nd}) is considerably higher in borates and other hosts compared to the present barium-alumino-metaphosphate glasses. As C_{DA}^{Nd-Nd} defines the energy lose by self-quenching among donors, it may limit the highest allowed doping concentration. For high power lasers or solar concentrators, effective

absorption is necessary, which demands high donor ion concentrations. At the same time, the energy loss due to self-quenching or multi-phonon relaxation should be less for efficient sensitized luminescence. The present barium-alumino-metaphosphate glasses possess least C_{DA}^{Nd-Nd} and a reasonable C_{DA}^{Nd-Yb}, which manifest their potential for high-energy laser applications. The least value of energy loss due to donor self-quenching in the present glass system is probably due to the long chain like metaphosphate network, which restricts the clustering even at high dopant concentrations. Based on the above considerations, a performance factor denoted by Φ_{ET} to quantify the sensitization ability per unit loss for different host materials has been evaluated using Eq. (8) and the values are tabulated in Table II. It is found to be highest for present barium-alumino-metaphosphate glasses suggesting their superiority over other reported host materials for $Nd^{3+} \rightarrow Yb^{3+}$ energy transfer.

D. $Nd^{3+} \leftarrow Yb^{3+}$ Energy Back-Transfer

In order to further establish the effective energy transfer between Nd^{3+} and Yb^{3+} in the barium-alumino-metaphosphate glasses, $Nd^{3+} \leftarrow Yb^{3+}$ energy back-transfer studies have been performed experimentally on codoped glasses by direct excitation of Yb^{3+} ions. Figure 9 presents the emission spectra of codoped samples upon excitation at 951 nm, which exhibits a weak Nd^{3+} emission at 1320 nm along with Yb^{3+} emission at 1 μm indicating energy back-transfer do exists at room temperature. An enlarged view in the inset shows a decrease in Nd^{3+} emission with an increase in Yb^{3+} concentration. Under direct excitation, the Yb^{3+} emission intensity demonstrate a continuous increase even for higher concentrations unlike on Nd^{3+} excitation at 806 nm, where it has exhibited a decrease above 3 mol% Yb_2O_3 concentration as shown in Fig. 2. In the later case, if the observed Yb^{3+} emission quenching is assumed to be due to $Nd^{3+} \leftarrow Yb^{3+}$ energy back-transfer, more quenching is expected for direct excitation compared to the Nd^{3+} excitation. However, the results are contradictory.

This excitation dependent behaviour of Yb^{3+} emission can be explained through the energy migration among Yb^{3+} ions. Under Nd^{3+} excitation at 806 nm, relatively more unexcited Yb^{3+} ions will be available for an excited Yb^{3+} ion compared to Yb^{3+} direct excitation at 951 nm and thus the migration effect will be more prominent on Nd^{3+} excitation than on Yb^{3+} excitation to cause the observed luminescence quenching. This has been further confirmed from the Yb^{3+} luminescence decay spectra as presented in Fig. 10. The decay time is almost constant for low Yb_2O_3 concentration, but it falls rapidly above 3 mol%, which may be due to the energy migration among Yb^{3+} ions as migration becomes significant at higher concentrations.

At Yb_2O_3 concentration as low as 0.05 mol%, the migration effect is assumed to be negligible and the decay profile of BAP-NdYb005 glass has been analysed using direct energy transfer based Inokuti-Hirayama model for the evaluation of $Nd^{3+} \leftarrow Yb^{3+}$ energy transfer microparameter. Figure 11(a) presents the decay profile of Yb^{3+} emission at 975 nm on excitation at 951 nm along with a theoretical fit generated using Eq. (4). The simulated fit is in excellent correlation with the experimental data giving an energy transfer microparameter, C_{AD}^{Yb-Nd} value equals to 7×10^{-42} $cm^6\,s^{-1}$. Such a small value of energy transfer microparameter is due to a meagre spectral overlap between Yb^{3+} emission and Nd^{3+} absorption as depicted in the Fig. 11(b). The spectral overlap integral gave a value of C_{AD}^{Yb-Nd} equals to 1.8×10^{-42} $cm^6\,s^{-1}$, which shows a notable deviation from the value obtained from decay analysis. This difference is due to the ambiguity in considering the phonon assistance for $Nd^{3+} \leftarrow Yb^{3+}$ energy back-transfer since it require anti-Stokes transitions, which are less probable at room temperature. However, the order of both the values are same and thus it can be concluded that the $Nd^{3+} \leftarrow Yb^{3+}$ energy back-transfer microparameter, C_{AD}^{Yb-Nd} ($\times 10^{-42}$ $cm^6\,s^{-1}$) is almost three order of magnitude less than the $Nd^{3+} \rightarrow Yb^{3+}$ energy transfer

microparameter, C_{DA}^{Nd-Yb} (× 10^{-39} $cm^6\,s^{-1}$) in presently reported barium-alumino-metaphosphate glasses.

5. CONCLUSIONS

In summary, we conclude that a new series of Nd^{3+} - Yb^{3+} codoped barium-alumino-metaphosphate glasses have been prepared and successfully studied for their energy transfer mechanisms. An efficient $Nd^{3+} \rightarrow Yb^{3+}$ energy transfer has been observed in the present glasses with the energy transfer efficiency reaching up to 95% for 9 mol% Yb_2O_3 concentration, which has been satisfactorily explained due to the effective contribution of host phonons. The Yb_2O_3 concentration of 3 mol% has been found to be an optimum content for sensitized Yb^{3+} luminescence; where Nd^{3+} emission has totally been quenched. The energy transfer analysis has revealed that the energy transfer mechanism is governed by hopping migration among donors (Nd^{3+}) before finally sensitising the acceptors (Yb^{3+}). The energy transfer microparameters for $Nd^{3+} \rightarrow Yb^{3+}$ energy transfer and $Nd^{3+} \leftarrow Yb^{3+}$ energy back-transfer have been estimated based on the application of the Forster's spectral overlap model and donor luminescence decay analysis using theoretical simulations, and are found to be 1.65 × 10^{-39} $cm^6\,s^{-1}$ and 1.8 - 7 × 10^{-42} $cm^6\,s^{-1}$ respectively indicating that the direct $Nd^{3+} \rightarrow Yb^{3+}$ energy transfer is almost three order greater than the $Nd^{3+} \leftarrow Yb^{3+}$ energy back-transfer in present glasses. Similarly, an attempt has been made to quantify the sensitisation ability per unit loss among donor-acceptors by introducing a performance factor defined as a ratio of $Nd^{3+} \rightarrow Yb^{3+}$ energy transfer microparameter to the Nd^{3+} - Nd^{3+} self-quenching microparameter. The value of which is found to be significantly encouraging for present Ba-Al-metaphosphate glasses demonstrating the potentiality of these glasses for their use in solar energy concentrators as well as for high-energy lasers.

ACKNOWLEDGMENTS

Authors would like to thank Prof. I. Manna, Director, CGCRI for his kind encouragement and permission to publish this work that was carried out in an In-house project No. OLP-0270. One of us (Mr.A.D.S.) is thankful to the BRNS-DAE for the award of Junior Research Fellowship to him.

REFERENCES

1. M. J. Weber, "Optical properties of Yb^{3+} and Nd^{3+}-Yb^{3+} energy transfer in $YAlO_3$," Phys. Rev. B **4**, 3153-3159 (1971).
2. R. Reisfeld and Y. kalisky, "Nd^{3+} and Yb^{3+} germanate and tellurite glasses for fluorescence solar energy collectors," Chem. Phys. Lett. **80**, 178-183 (1981).
3. D. Jaque, M. O. Ramirez, L. E. Bausà, J. García Solé, E. Cavalli, A. Speghini and M. Bettinelli, " $Nd^{3+} \rightarrow Yb^{3+}$ energy transfer in $YAl_3(BO_3)_4$ nonlinear laser crystal," Phys. Rev. B **68**, 035118-1 - 9 (2003).
4. F. Liégard, J. L. Doualan, R. Moncorgé and M. Bettinelli, "$Nd^{3+} \rightarrow Yb^{3+}$ energy transfer in a codoped metaphosphate glass as a model for Yb^{3+} laser operation around 980 nm," Appl. Phys. B **80**, 985-991 (2005).
5. D. F. De Sousa, F. Batalioto, M. J. V. Bell, S. L. Oliveira and L. A. O. Nunes, "Spectroscopy of Nd^{3+} and Yb^{3+} codoped fluoroindogallate glasses," J. Appl. Phys. **90**, 3308-3313 (2001).
6. R. Balda, J. Fernàndez, I. Iparraguirre and M. Al-Saleh, "Spectroscopic study of Nd^{3+}/Yb^{3+} in disordered potassium bismuth laser crystals," Opt. Mater. **28**, 1247-1252 (2006).

7. Z. Jia, A. Arcangeli, X. Tao, J. Zhang, C. Dong, M. Jiang, L. Bonelli and M. Tonelli, "Efficient $Nd^{3+} \rightarrow Yb^{3+}$ energy transfer in Nd^{3+}, Yb^{3+}: $Gd_3Ga_5O_{12}$ multicenter garnet crystal," J. Appl. Phys. **105**, 083113-1-6 (2009).

8. X. Zou and T. Izumitani, " Excitation energy transfer of Nd^{3+} - Yb^{3+} - Er^{3+} in several glasses," J. Ceram. Soc. Jpn. **101**, 84-88 (1993).

9. C. Lurin, C. Parent, G. Le Flem and P. Hagenmuller, "Energy transfer in a Nd^{3+} - Yb^{3+} borate glass," J. Phys. Chem. Solids **46**, 1083-1092 (1985).

10. U. Caldinõ, D. Jaque, E. Martín-Rodríguez, M. O. Ramírez, J. García Solé, A. Speghini and M. Bettinelli, "$Nd^{3+} \rightarrow Yb^{3+}$ resonant energy transfer in the ferroelectric $Sr_{0.6}Ba_{0.4}Nb_2O_6$ laser crystal," Phys. Rev. B **77**, 075121-1-8 (2008).

11. A. Lupei, V. Lupei and A. Ikesue, C. Gheorghe, "Spectroscopic and energy transfer investigation of Nd/Yb in Y_2O_3 transparent ceramics," J. Opt. Soc. Am. B **27**, 1002-1010 (2010).

12. G. L. Bourdet, O Casagrande, N. Deguil-Robin and B. Le Garrec, "Performances of cryogenic cooled laser based on Ytterbium doped sesquioxide ceramics," J. Phys.: Conf. Ser **112**, 032054-1 - 4 (2008).

13. V V Ovchinnikov, A K Murtazaev, E. A. Khazanov and A. M. Sergeev, "Equilibrium and highly nonequilibrium states of condensed matter," Phys.-Usp. **51**, 955-974 (2008).

14. D. Jaque, M. O. Ramirez, L. E. Bausà, A. Speghini, M. Bettinelli and E. Cavalli, "Influence of Nd^{3+} and Yb^{3+} concentration on the $Nd^{3+} \rightarrow Yb^{3+}$ energy-transfer efficiency in the $YAl_3(BO_3)_4$ nonlinear crystal: determination of optimum concemtration for lasert applications," J. Opt. Soc. Am. B **21**, 1203-1209 (2004).

15. M. O. Ramirez, D. Jaque, L. E. Bausà, I. R. Martin, F. Lahoz, E. Cavalli, A. Speghini and M. Bettinelli, "Temperature dependence of $Nd^{3+} \leftrightarrow Yb^{3+}$ energy transfer in the $YAl_3(BO_3)_4$ nonlinear laser crystal," J. Appl. Phys. **97**, 093510-1-8 (2005).
16. A. Matic, L. Börgesson, A. Wannberg and R. L. McGreevy, "Structural studies of rare-earth doped phosphate glasses," Mat. Res. Soc. Symp. Proc. **455**, 435-440 (1997).
17. A. D. Sontakke, K. Biswas, A. K. Mandal and K. Annapurna, "Concentration quenched luminescence and energy transfer analysis of Nd^{3+} doped Ba-Al-metaphosphate laser glasses," Appl. Phys. B **101**, 235-244 (2010).
18. D. L. Dexter, "A theory of sensitized luminescence in solids," J. Chem. Phys. **21**, 836-850 (1953).
19. M. Inokuti and F. Hirayama, "Influence of energy transfer by the exchange mechanism on donor luminescence," J. Chem. Phys. **43**, 1978-1989 (1965)
20. J. A. Caird, A. J. Ramponi and P. R. Staver, "Quantum efficiency and excited-state relaxation dynamix in Neodymium-doped phosphate laser glasses," J. Opt. Soc. Am. B **8**, 1391-1403 (1991).
21. F. Auzel, "Multiphonon assisted and anti-Stokes and Stokes fluorescence of triply ionized rare-earth ions," Phys. Rev. B **13**, 2809-2817 (1976).
22. M. C. Nostrand, R. H. Page, S. A. Payne, L. I. Isaenko and A. P. Yelisseyev, "Optical properties of Dy^{3+}- and Nd^{3+} -doped KPb_2Cl_5," J. Opt. Soc. Am. B **18**, 264-276 (2001).
23. E. Yahel, O. Hess and A. A. Hardy, "Modeling and optimization of high-power Nd^{3+}-Yb^{3+} codoped fiber lasers," J. Lightwave Tech. **24**, 1601-1609 (2006).

24. P. Y. Shih, J. Y. Ding and S. Y. Lee, "^{31}P MAS-NMR and FTIR analyses on the structure of CuO-containing sodium poly-and Metaphosphate glasses," Mater. Chem. Phys. **80**, 391-396 (2003).

25. A. D. Sontakke, K. Biswas, A. K. Mandal and K. Annapurna, "Time resolved fluorescence and energy transfer analysis of Nd^{3+} - Yb^{3+} - Er^{3+} triply doped Ba-Al-metaphosphate glasses of an eye safe emission (1.54 μm)," J. Fluoresc. **20**, 425-434 (2010).

26. C. Parent, C. Lurin, G. Le Flem and P. Hagenmuller, "$Nd^{3+} \rightarrow Yb^{3+}$ energy transfer in glasses with composition close to $LiLnP_4O_{12}$ metaphosphate (Ln = La, Nd, Yb)," J. Lumin. **36**, 49-55 (1986).

27. D. Jaque, J. A. Muñoz, F. Cussó and J. Garcia Solé, "Quantum efficiency of the $YAl_3(BO_3)_4$:Nd self-frequency-doubling laser material," J. Phys.: Condens. Matter **10**, 7901-7905 (1998).

28. V. Lupei, A. Lupei, C. Gheorghe, S. Hau and A. Ikesue, "Efficient sensitization of Yb^{3+} emission by Nd^{3+} in Y_2O_3 transparent ceramics and the prospect for high-energy lasers," Opt. Lett. **34**, 2141-2143 (2009).

29. W. Ryba-Romanowsky, S. Golab, L. Cichosz and B. Jeżowska,-Trzebiatowska, "Influence of temperature and acceptor concentration on energy transfer from Nd^{3+} to Yb^{3+} and from Yb^{3+} to Er^{3+} in tellurite glass," J. Non-Cryst. Solids **105**, 295-302 (1988).

30. B. I. Denker, V. V. Osiko, P. P. Pashinin, A. M. Prokhorov, "Concentrated neodymium laser glasses (review)," Sov. J. Quantum Electron. **11,** 289-296 (1981).

Table Captions

Table 1. Fluorescence decay time (τ), energy transfer rate (W_{ET}) and energy transfer efficiency (η_{ET}) of different Nd^{3+} - Yb^{3+} codoped Ba-Al-metaphosphate glasses.

Table 2. Energy transfer microparameter (C_{DA}^{Nd-Yb}) for $Nd^{3+} \rightarrow Yb^{3+}$ energy transfer, Nd^{3+} - Nd^{3+} self-quenching microparameter (C_{DA}^{Nd-Nd}) and performance factor (Φ_{ET}) for different hosts.

Figure Captions

Fig. 1. Optical absorption spectra of Nd^{3+} - Yb^{3+} codoped Ba-Al-metaphosphate glasses.

Fig. 2. Photoluminescence spectra of Nd^{3+} - Yb^{3+} codoped Ba-Al-metaphosphate glasses with 806 nm excitation. (Inset: Plot of emission intensity of Nd^{3+} and Yb^{3+} as a function of Yb_2O_3 concentration)

Fig. 3. Spectral overlap of Nd^{3+} emission ($^4F_{3/2} \rightarrow {}^4I_{9/2}$) with Yb^{3+} absorption ($^2F_{7/2} \rightarrow {}^2F_{5/2}$) cross sections. Inset : Partial energy level diagram of Nd^{3+} and Yb^{3+} ions in Ba-Al-metaphosphate glasses.

Fig. 4. (a) Plot of energy transfer probability (P_{ET}) as a function of phonon energy (E_{ph}). (b) FTIR reflectance spectrum of Ba-Al-metaphosphate glass.

Fig. 5. Variation of $Nd^{3+} \rightarrow Yb^{3+}$ energy transfer efficiency with Yb_2O_3 concentration in Ba-Al-metaphosphate glasses.

Fig. 6. Normalized fluorescence decay profiles of Nd^{3+} ions.

Fig. 7. Spectral overlap of Nd^{3+} emission cross section and Yb^{3+} absorption cross section with respective phonon side bands.

Fig. 8. Normalized fluorescence decay spectrum of Nd^{3+} emission in BAP-NdYb05 glass with theoretical fit generated using Burshtein's hopping model.

Fig. 9. Photoluminescence spectra of Nd^{3+}-Yb^{3+} codoped Ba-Al-metaphosphate glasses on Yb^{3+} excitation at 951 nm. (Inset: Enlarged view of $^4F_{3/2} \rightarrow {}^4I_{13/2}$ emission transition of Nd^{3+})

Fig. 10. Normalized fluorescence decay profiles of Yb^{3+} ions.

Fig. 11. (a) Normalized fluorescence decay profiles of Yb^{3+} emission in BAP-NdYb005 glass with theoretical fit generated using Inokuti-Hirayama model. (b) Spectral overlap of Yb^{3+} emission ($^2F_{5/2} \rightarrow {}^2F_{7/2}$) and Nd^{3+} absorption ($^4I_{9/2} \rightarrow {}^4F_{3/2}$) cross sections.

Table 1

Glass	τ **(µsec)**	W_{ET} **(sec^{-1})**	η_{ET}
BAP-Nd	283.6	-	-
BAP-NdYb005	253.3	422.1	10.7
BAP-NdYb01	238.2	672.5	16.0
BAP-NdYb05	147.8	3240.5	47.9
BAP-NdYb10	101.5	5952.2	64.2
BAP-NdYb30	38.3	22606.8	86.5
BAP-NdYb60	19.3	48287.4	93.2
BAP-NdYb90	14.1	66355.1	95.1

Table 2

Host	C_{DA}^{Nd-Yb} **(cm^6 s^{-1})**	C_{DA}^{Nd-Nd} **(cm^6 s^{-1})**	Φ_{ET}	**Reference**
$YAl_3(BO_3)_4$ crystal	18×10^{-39}	-	-	[3]
Borate glass	6×10^{-39}	1.6×10^{-39}	3.75	[9]
Y_2O_3 transparent ceramics	5×10^{-39}	1.75×10^{-39}	2.86	[28]
Telluride glass	3.4×10^{-39}	0.55×10^{-39}	6.18	[29]
Pb-ultraphosphate glass	2.4×10^{-39}	-	-	[9]
$Gd_3Ga_5O_{12}$ crystal	2.1×10^{-39}	-	-	[7]
Li-La metaphosphate glass	1.6×10^{-39}	0.03×10^{-39} (77K)	53.33	[26, 30]
$K_5Bi(MoO_4)_4$ crystal	1.34×10^{-39}	-	-	[6]
$Sr_{0.6}Ba_{0.4}Nb_2O_6$ crystal	0.56×10^{-39}	-	-	[10]
Fluoroindogallate glass	0.3×10^{-39}	0.25×10^{-39}	1.2	[5]
Ba-Al-metaphosphate glass	1.65×10^{-39}	0.004×10^{-39}	412.5	Present work

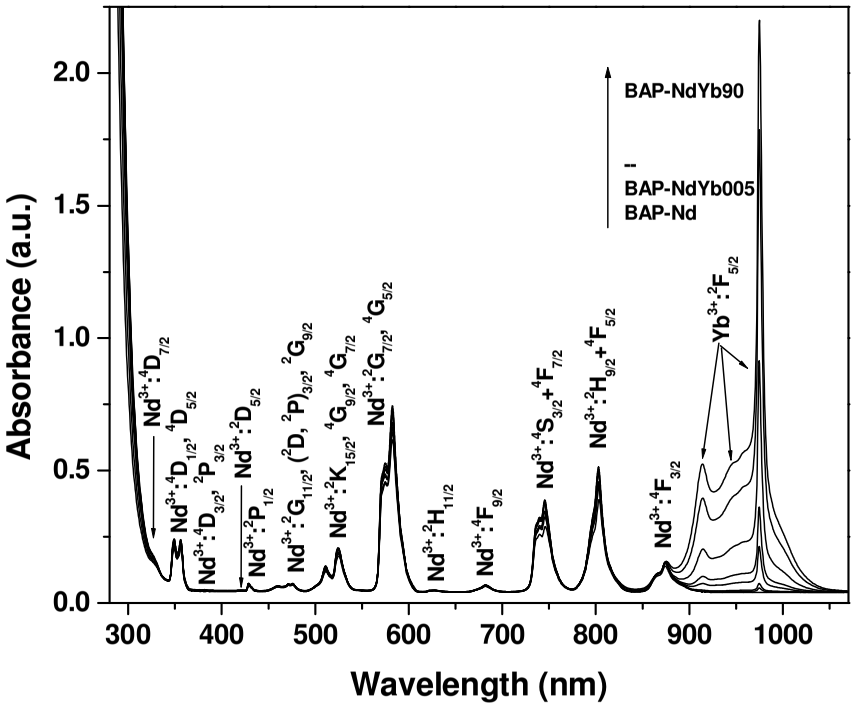
Absorbance (a.u.)
Wavelength (nm)
BAP-NdYb90
BAP-NdYb005
BAP-Nd
Nd3+:4D7/2
Nd3+:4D1/2, 4D5/2
Nd3+:4D3/2, 2P3/2
Nd3+:2P1/2
Nd3+:2D5/2
Nd3+:2G11/2, (2D, 2P)3/2, 2G9/2
Nd3+:2K15/2, 4G9/2, 4G7/2
Nd3+:2G7/2, 4G5/2
Nd3+:2H11/2
Nd3+:4F9/2
Nd3+:4S3/2+4F7/2
Nd3+:2H9/2+4F5/2
Nd3+:4F3/2
Yb3+:2F5/2

Fig. 1

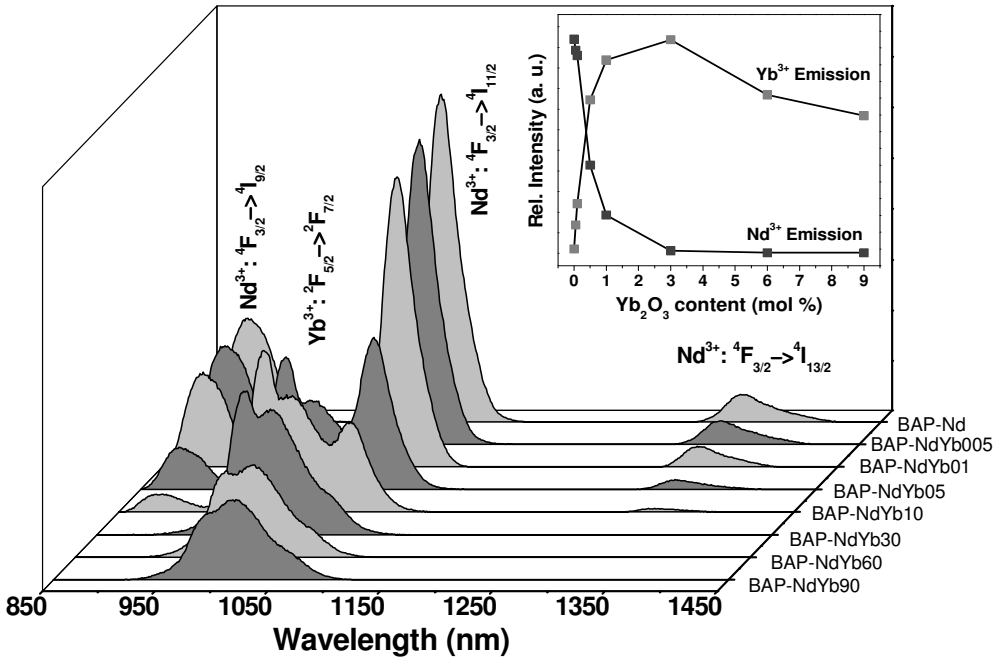
Nd3+: 4F3/2 –> 4I9/2
Yb3+: 2F5/2 –> 2F7/2
Nd3+: 4F3/2 –> 4I11/2
Nd3+: 4F3/2 –> 4I13/2
Rel. Intensity (a. u.)
Yb3+ Emission
Nd3+ Emission
0 1 2 3 4 5 6 7 8 9
Yb2O3 content (mol %)
BAP-Nd
BAP-NdYb005
BAP-NdYb01
BAP-NdYb05
BAP-NdYb10
BAP-NdYb30
BAP-NdYb60
BAP-NdYb90
850 950 1050 1150 1250 1350 1450
Wavelength (nm)

Fig. 2

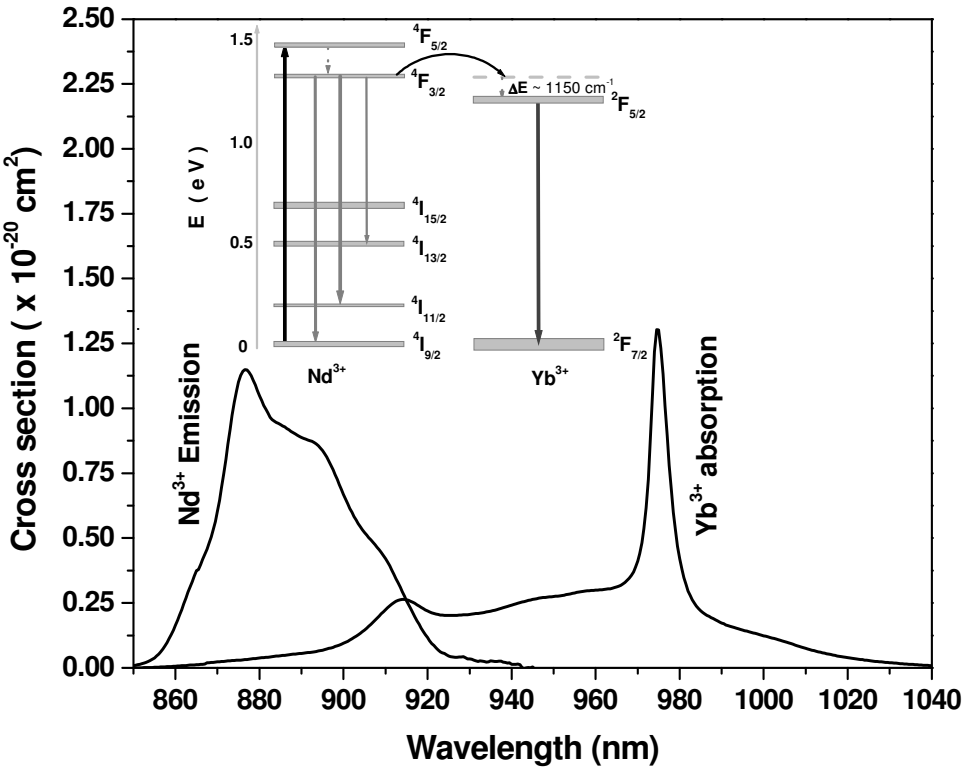
Cross section (x 10^{-20} cm^2)
Wavelength (nm)
Nd^{3+} Emission
Yb^{3+} absorption
E (e V)
$^4F_{5/2}$
$^4F_{3/2}$
$^4I_{15/2}$
$^4I_{13/2}$
$^4I_{11/2}$
$^4I_{9/2}$
ΔE ~ 1150 cm^{-1}
$^2F_{5/2}$
$^2F_{7/2}$
Nd^{3+}
Yb^{3+}

Fig. 3

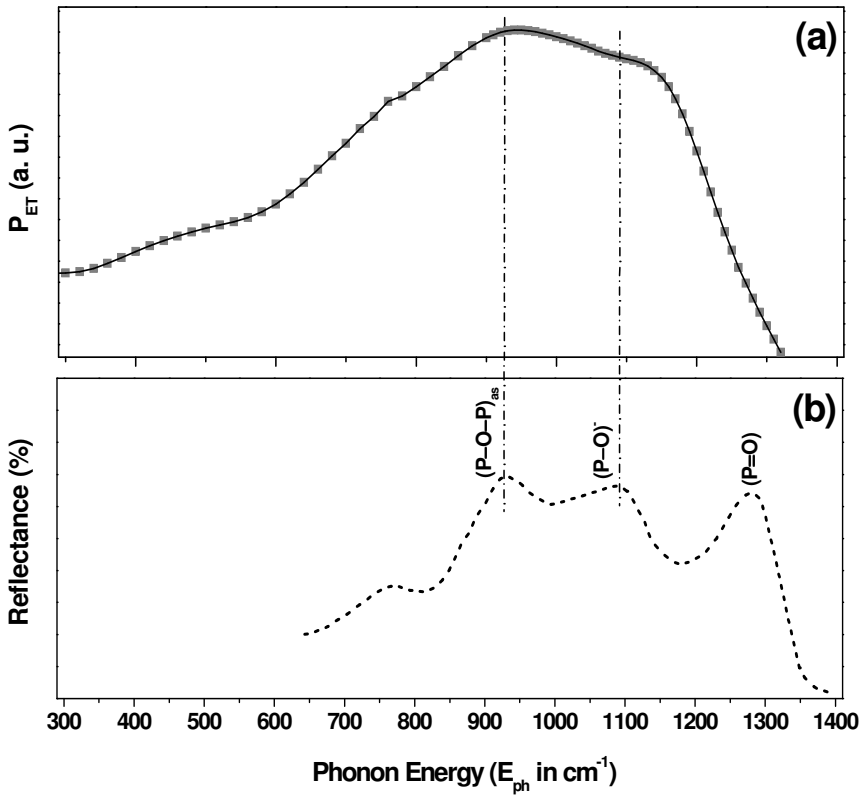
(a)
(b)
P_{ET} (a. u.)
Reflectance (%)
$(P–O–P)_{as}$
$(P–O)^{-}$
(P=O)
300
400
500
600
700
800
900
1000
1100
1200
1300
1400
Phonon Energy (E_{ph} in cm^{-1})

Fig. 4

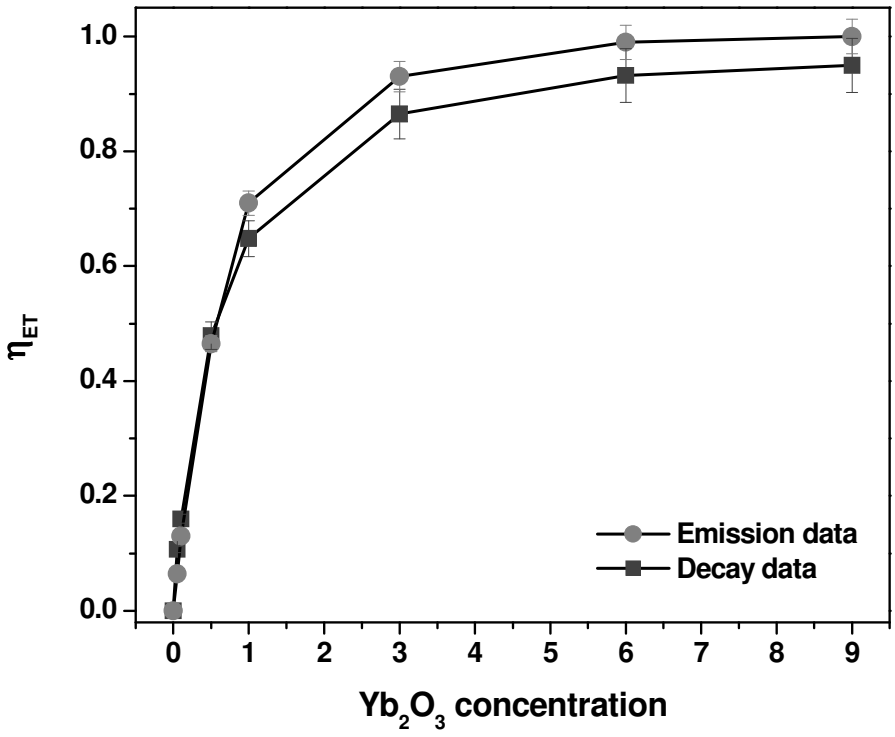
1.0
0.8
0.6
0.4
0.2
0.0
η_{ET}
0
1
2
3
4
5
6
7
8
9
Yb_2O_3 concentration
Emission data
Decay data

Fig. 5

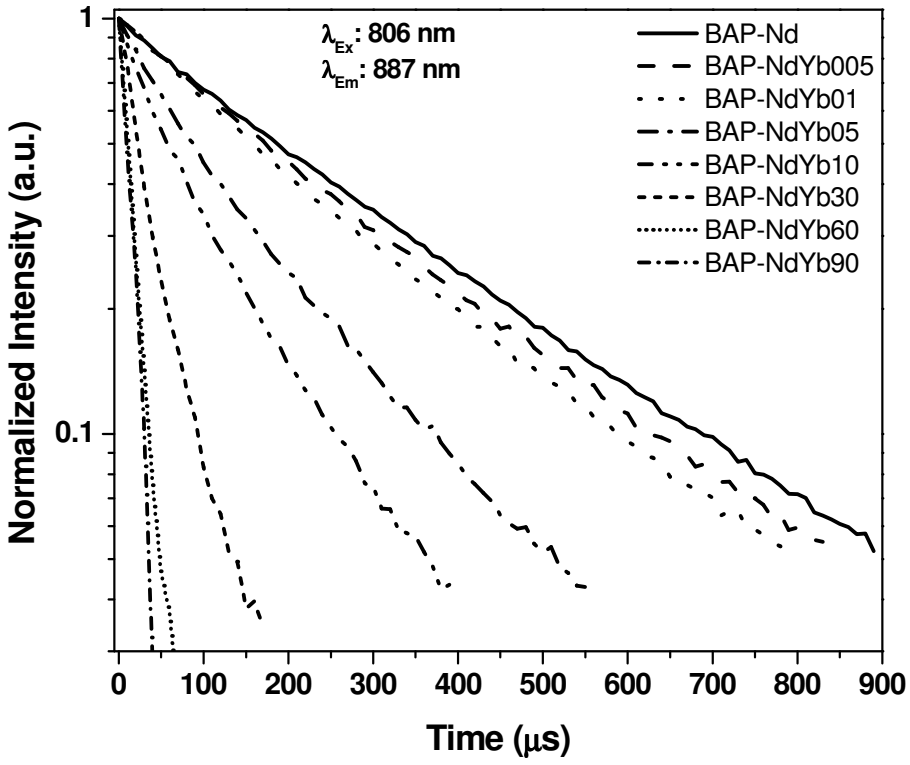
λEx: 806 nm
λEm: 887 nm
BAP-Nd
BAP-NdYb005
BAP-NdYb01
BAP-NdYb05
BAP-NdYb10
BAP-NdYb30
BAP-NdYb60
BAP-NdYb90
Normalized Intensity (a.u.)
1
0.1
0
100
200
300
400
500
600
700
800
900
Time (μs)

Fig. 6

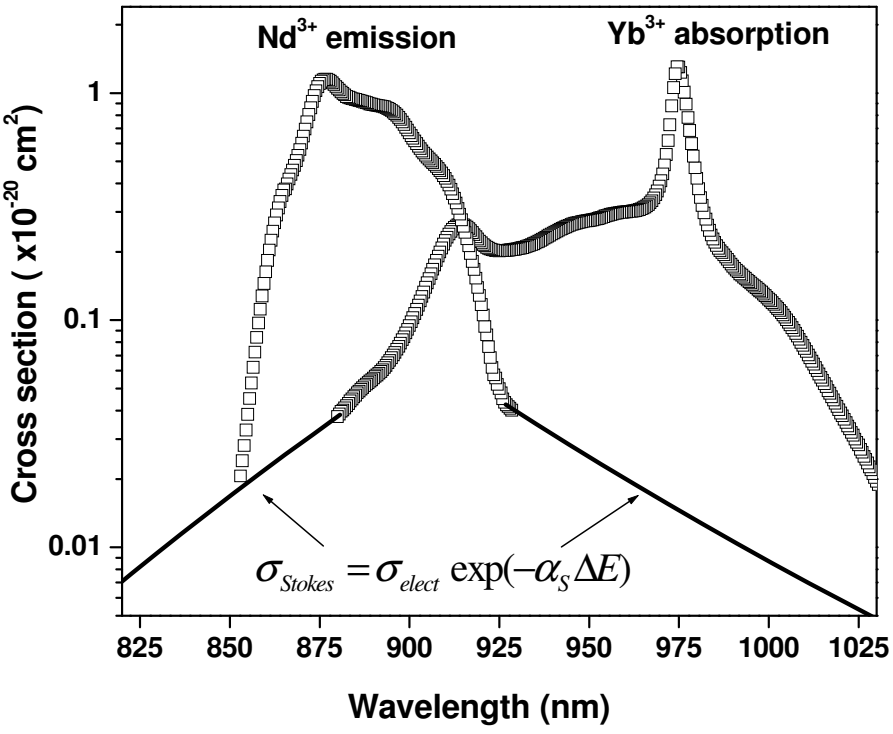
Nd3+ emission
Yb3+ absorption
Cross section (x10-20 cm2)
1
0.1
0.01
σStokes = σelect exp(−αSΔE)
825
850
875
900
925
950
975
1000
1025
Wavelength (nm)

Fig. 7

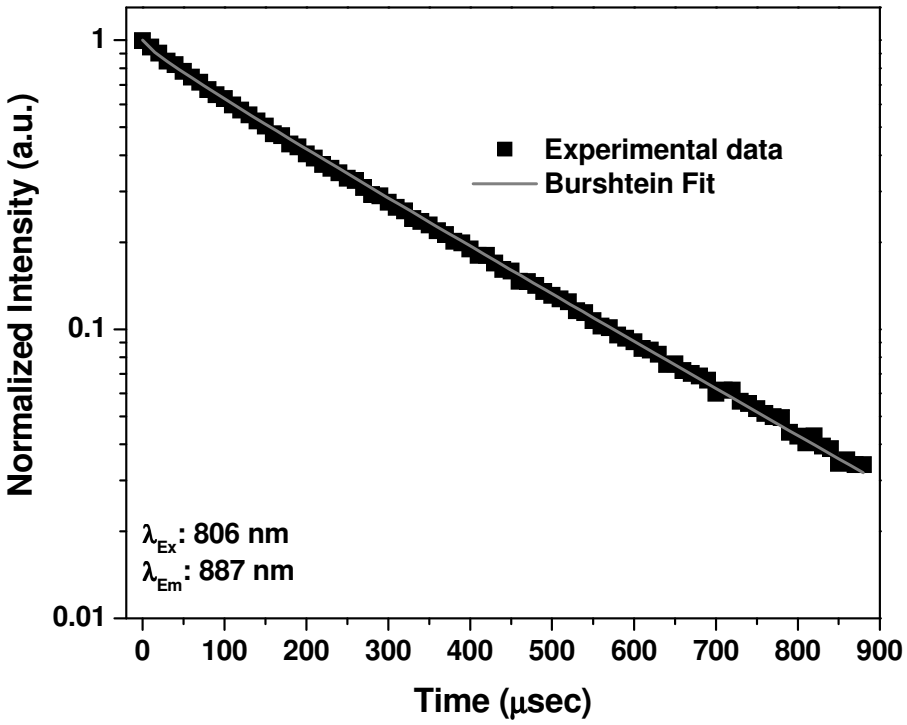
Normalized Intensity (a.u.)
1
0.1
0.01
0
100
200
300
400
500
600
700
800
900
Time (μsec)
Experimental data
Burshtein Fit
λEx: 806 nm
λEm: 887 nm

Fig. 8

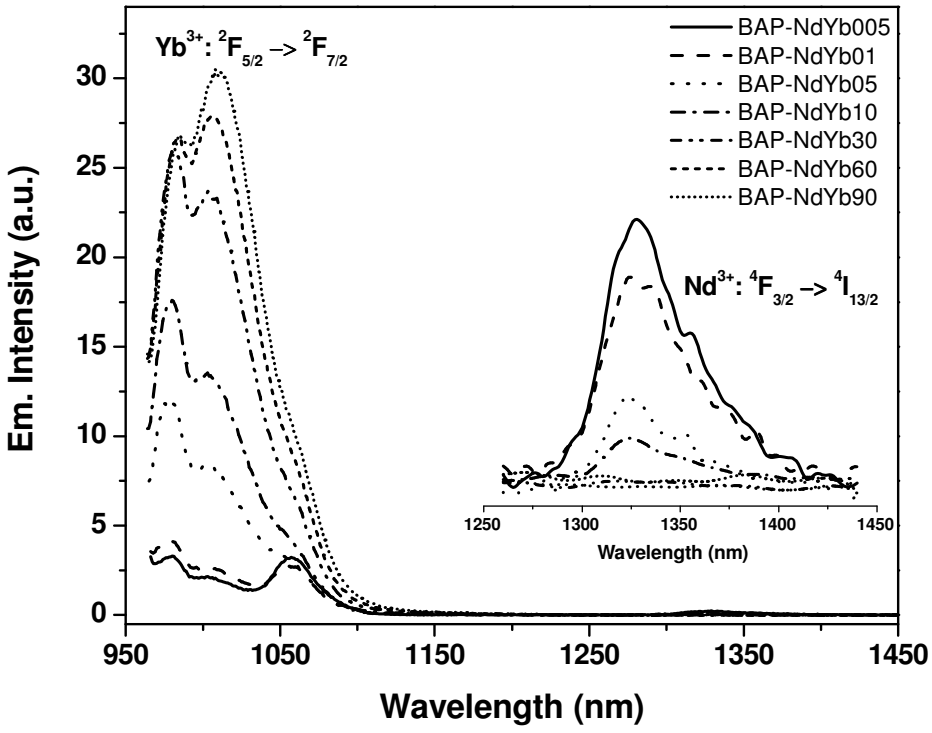
Yb3+: 2F5/2 -> 2F7/2
BAP-NdYb005
BAP-NdYb01
BAP-NdYb05
BAP-NdYb10
BAP-NdYb30
BAP-NdYb60
BAP-NdYb90
Nd3+: 4F3/2 -> 4I13/2
Em. Intensity (a.u.)
Wavelength (nm)
0
5
10
15
20
25
30
950
1050
1150
1250
1350
1450
1250
1300
1350
1400
1450

Fig. 9

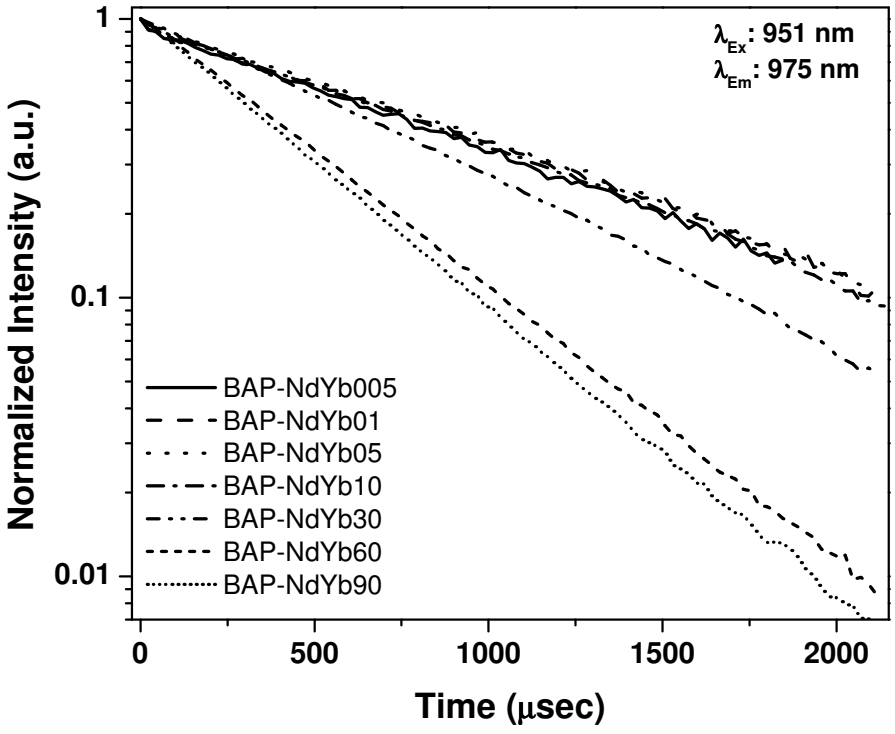
λEx: 951 nm
λEm: 975 nm
Normalized Intensity (a.u.)
1
0.1
0.01
0
500
1000
1500
2000
Time (μsec)
BAP-NdYb005
BAP-NdYb01
BAP-NdYb05
BAP-NdYb10
BAP-NdYb30
BAP-NdYb60
BAP-NdYb90

Fig. 10

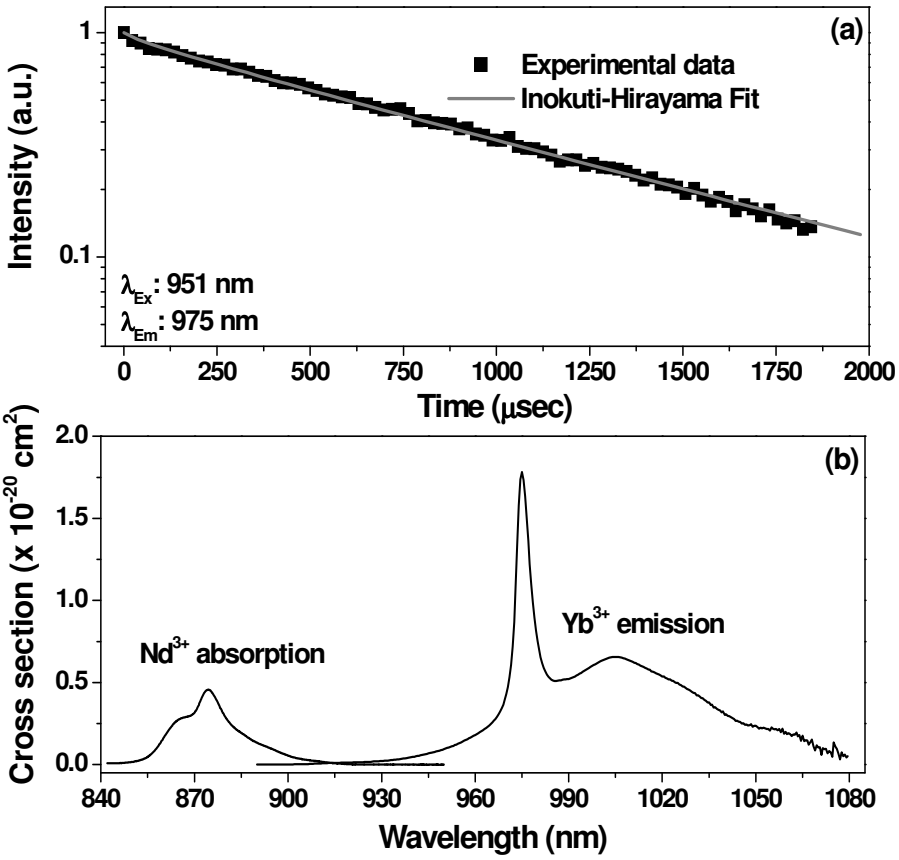
(a)
Experimental data
Inokuti-Hirayama Fit
Intensity (a.u.)
1
0.1
λEx: 951 nm
λEm: 975 nm
0
250
500
750
1000
1250
1500
1750
2000
Time (μsec)
(b)
Cross section (x 10-20 cm2)
2.0
1.5
1.0
0.5
0.0
Nd3+ absorption
Yb3+ emission
840
870
900
930
960
990
1020
1050
1080
Wavelength (nm)

Fig. 11